ADVANCED MATERIALS INTERFACES
www.advmatinterfaces.de

Size-Dependent Catalytic Behavior of Gold Nanoparticles

*Chen Liang, Jun Young Cheong, Gabriel Sitaru, Sabine Rosenfeldt, Anna S. Schenk, Stephan Gekle, Il-Doo Kim, and Andreas Greiner**

Gold nanoparticles (AuNP) are widely used for reaction catalysis. The common understanding is that the smaller the particles, the more reactive they are. It is reported here that this is not always the case for citrate (Ct) or polyvinylpyrrolidone (PVP) stabilized AuNP in the catalytic reduction of 4-nitrophenol with sodium borohydride ($NaBH_4$), when the total surface area is kept constant. The results prove that for AuNP in the size range of 10–58 nm, the reactivity increases with increasing particle diameter for the investigated model reaction. The trend of catalytic activity is independent of the conjugated ligands for citrate and PVP ligands. Purely based on size and resulting surface area, the trend in catalytic activity is unexpected. Only a more detailed structural investigation revealed that internal structure parameters like defect tendency also play a strong role. Larger AuNP possess more defects between crystalline domains. Further, the influence of the ligand density on the surface of AuNP and the diffusion effect of reactants are excluded for the nitrophenol reduction.

1. Introduction

Over the last two decades, AuNP have attracted significant attention in many application areas, such as biomedical applications,[1] sensors,[2] and photonics.[3] AuNP have also been proven to hold great potential in catalysis.[4] AuNP have been widely synthesized and investigated as the catalyst in various reactions, such as CO oxidation,[5] aerobic oxidation of alcohols,[6] hydrogenation,[7] coupling reactions,[8] and reductive reactions.[9] AuNP present excellent performance in high catalytic activities, simple purification, easy recovery, and recyclability, all extensively used in industrial applications. As a classic model reaction, the reductive reaction of nitrophenol to aminophenol with the help of sodium borohydride ($NaBH_4$) has often been utilized to evaluate the catalytic activities of AuNP.[10] Previous studies reported that the size,[11] shape,[12] and capping ligands[13] of AuNP play essential roles in catalytic activities and are crucial factors determining the reaction rate. For example, Fenger's work demonstrated that 13 nm CTAB capped AuNP presented the highest catalytic activity for nitrophenol reduction if the size of the AuNP is between 3.5 and 56 nm.[11b] Zboril and co-workers proved that gold nanoparticles with decreasing size presented increasing catalytic activity for the same reaction.[14] It has been demonstrated that smaller particles are much more active than bigger particles because they provide a higher surface area. To the best of our knowledge, only very few literatures have been published on the influence of the size of AuNP with the same total surface areas (i.e., $\Sigma N_i A_i = \Sigma N_j A_j$, N_i, N_j are the number of particles i and j, respectively and A_i, A_j represent surface area of the single nanoparticle i and j) but different particle diameters on the nitrophenol reductive reaction. For example, Puntes et al. described that if the AuNP possess well-controlled decahedral morphology,[11e] the activity of the AuNP decreases with increasing size. It was proposed that gold atoms are lower coordinated on the smaller nanoparticle than on the bigger ones.

This work aims to provide new insights into the influence of the surface area and structure of AuNP on their catalytic behavior by a detailed study from a different perspective. For this purpose, the catalytic nitrophenol reduction was carried out with AuNP of various sizes. The condition was that the total surface areas of AuNP of different sizes were kept the same. To bring the finding on broader data basis, the experiments were performed with two different capping ligands, citrate (Ct) and polyvinylpyrrolidone (PVP).

C. Liang, A. Greiner
Department of Macromolecular Chemistry
University of Bayreuth, Bavarian Polymer Institute
Universitätsstrasse 30, 95440 Bayreuth, Germany
E-mail: greiner@uni-bayreuth.de
J. Y. Cheong, I.-D. Kim
Department of Materials Science and Engineering
Korea Advanced Institute of Science and Technology (KAIST)
Daejeon 34141, Republic of Korea
G. Sitaru, S. Gekle
Biofluid Simulation and Modeling Department
University of Bayreuth
Theoretische Physik VI
Universitätsstrasse 30, 95440 Bayreuth, Germany
S. Rosenfeldt
Physical Chemistry I and Bavarian Polymer Institute
University of Bayreuth
Universitätsstrasse 30, 95440 Bayreuth, Germany
A. S. Schenk
Physical Chemistry – Colloidal Systems
University of Bayreuth
Bavarian Polymer Institute
Universitätsstrasse 30, 95440 Bayreuth, Germany
The ORCID identification number(s) for the author(s) of this article can be found under https://doi.org/10.1002/admi.202100867.

DOI: 10.1002/admi.202100867

2. Results and Discussion

The AuNP were synthesized by the traditional Frens method[15] with some modifications.[11a] AuNP of different sizes were synthesized by controlling the ratio between chloroauric acid ($HAuCl_4$) and sodium citrate (Na_3Ct). An excessive amount of sodium citrate was used during the synthetic process to eliminate the effect of the unreactive $HAuCl_4$. Based on these measures, 10 to 58 nm citrate capped spherical AuNP (Ct@AuNP) were prepared (Table S1, Supporting Information). The size of AuNP decreases with increasing ratio of $Na_3Ct/HAuCl_4$ as observed by transmission electron microscopy (TEM) (Figures S1 and S2, Supporting Information). The red-shifted UV–vis absorption spectra of Ct@AuNP also implied that the size of AuNP increases with decreasing ratio of $Na_3Ct/HAuCl_4$ (Table S1, Supporting Information). In addition, the size of AuNP obtained by dynamic light scattering (DLS) is in good agreement with the TEM data (Table S1, Supporting Information). For the PVP capped AuNP (PVP@AuNP), the particles with sizes ranging from 10 to 58 nm were obtained via the ligand exchange method from the Ct@AuNP. The PVP@AuNP presented the same size distribution and morphology as the pre-synthesized Ct@AuNP (Figure S3, Supporting Information). To prove the occurrence of ligand exchange, UV–vis absorption spectroscopy and ζ potential analysis of the PVP@AuNP were performed before and after ligand exchange. A slight red shift in the UV–vis absorption spectroscopy can be observed due to the higher molecular weight of the PVP compared to the citrate (Table S2, Supporting Information). The ζ potentials of the Ct@AuNP of different sizes are negative and in the range of −30.0 to −44.5 mV, which was attributed to the adsorption of the citrate on the surface of the AuNP (Table S1, Supporting Information). After ligand exchange the ζ potentials of the PVP@AuNP are in the range of −25.4 to −37.5 mV (Table S2, Supporting Information). The results indicate that PVP@AuNP has a slightly lower ζ potential than the corresponding Ct@AuNP of the same size. Even if PVP is not negatively charged, the experimental determined zeta potential is negative. This is counterintuitive but in good agreement with literature and may hint to partial ligand exchange.[16] Another proof of the successful ligand exchange can be the change of the colloidal stability from Ct@AuNP to PVP@AuNP with the later being more stable (less aggregation and sedimentation). A dramatic red shift of the absorption peak in the UV–vis spectra of Ct@AuNP can be observed after the addition of 0.3 M NaCl, whereas the spectra of the PVP@AuNP remained the same before and after addition of the 0.3 M NaCl. (Table S2 and Figure S4, Supporting Information).

The determination of the total area of the AuNP is of high importance. The total area is defined as $\Sigma N_i A_i$ (i represents a certain AuNP in an ensemble, A_i is the surface area of a certain shape (e.g., sphere, cylinder), and N_i is the number of AuNP with that shape) (Figure S5, Supporting Information). For example, A_i is $4\pi R^2$ for a sphere with a radius of R and $2\pi R^2 + 2\pi RL$ for a cylinder with a radius of R and a length of L. The kinetic study assumes that the small and big AuNP have on average identical total surface areas. Even if AuNP are expected to be spherical on average, derivation from this ideal shape becomes more likely with increasing size (Figure S2, Supporting Information). To get a measure of the limits of a spherical approximation, small-angle X-ray scattering (SAXS) as a volume-sensitive method was performed on a diluted 42 nm AuNP colloidal solution and a more concentrated colloidal solution of 10 nm AuNP (Figure S6, Supporting Information). Experimental data of both colloidal solutions could be described with a model of spherical particles (with a Gaussian size distribution). In detail, sizes of $2R_{SAXS}$ = 11.2 ± 1 nm and $2R_{SAXS}$ = 31.6 ± 4.8 nm for the small and large AuNP were obtained (solid lines in Figure S6, Supporting Information). Thus, we assumed that the average particles are spherical enough to apply the equations (Figure S5, Supporting Information).

Additionally, we determined the longest particle dimension by TEM analysis (measuring the longest axis L of at least 100 particles) and it was then utilized in the equations (Figure S5, Supporting Information). We are convinced that this averaged value, when inserted into equation given in Figure S5 in the Supporting Information, will enable estimation of the errors (maximum deviation) of the experimentally determined rate constant k. The TEM analysis led to values of 10 and 42 nm, respectively. Therefore, for the bigger AuNP the kinetic experiments were performed under UV–vis monitoring and the results were evaluated in two different ways, i.e., based on the total area of the NP determined either from TEM or from SAXS measurements leading to k_{TEM} (reaction rate constant based on TEM-derived NP size) and k_{SAXS} (reaction rate constant based on SAXS-derived NP size) (Tables S3 and S4, Supporting Information).

The reduction of 4-nitrophenol was selected as a model reaction due to its facile catalytic condition without side reactions. Further, this reaction can be easily monitored by UV–vis spectroscopy.[17] The equations in Figure S5 in the Supporting Information were utilized to calculate the mass of gold required to be employed in the 4-nitrophenol reductive reaction. The content of Au species in AuNP was determined by inductively coupled plasma optical emission spectroscopy (ICP-OES). The utilized mass of gold species is shown in Table S3 in the Supporting Information.

The color of the solution of nitrophenol changed from light yellow to dark yellow immediately after the addition of $NaBH_4$, which came along with a change of the characteristic absorption peak of the 4-nitrophenolate ions at 400 nm. Representative UV–vis spectra of the reductive procedure with time (**Figure 1**a) describe the change of UV–vis optical spectra of 4-nitrophenol reduction using 10 nm Ct@AuNP. A gradual decay of the characteristic peak at 400 nm and an emerging peak around 300 nm can be observed due to the generation of aminophenolate. As an excessive amount of $NaBH_4$ was employed in the experiment, the reaction condition can be regarded as pseudo first-order. The apparent reaction rate constant k (e.g., k_{SAXS} and k_{TEM}) of the reduction of 4-nitrophenol by $NaBH_4$ with the help of the gold catalyst can be described by the following equation [18]

$$-\ln\frac{C_t}{C_0} = -\ln\frac{A_t}{A_0} = kt \quad (1)$$

where k is the apparent reaction rate constant, t is the reaction time, C_t, and C_0 represent the concentrations of the nitrophenol

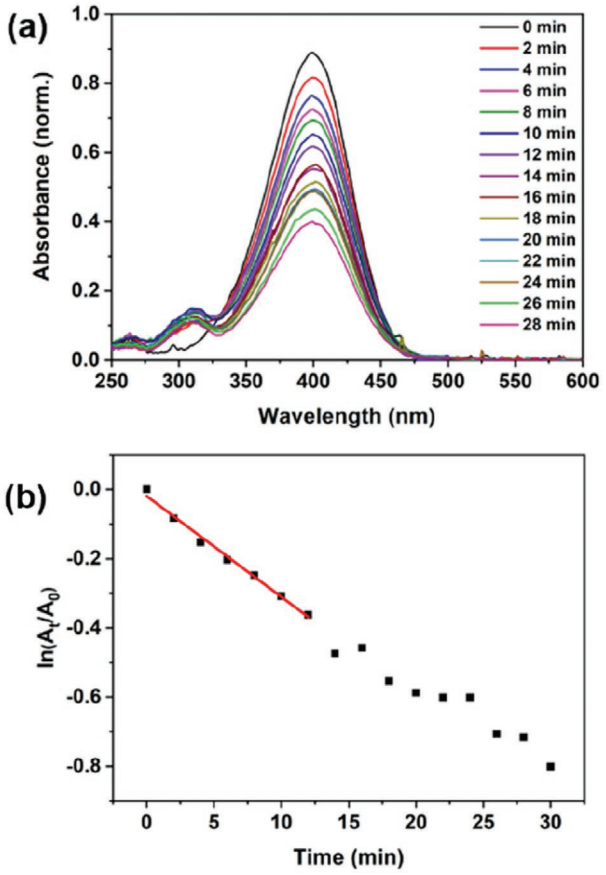

Figure 1. Kinetic study assuming a kinetic of pseudo-first-order. a) UV–vis spectral change of 4-nitrophenol reduction using 10 nm Ct@AuNP catalyst versus the time. b) The corresponding linear fitting of the UV–vis spectral change of 4-nitrophenol using 10 nm Ct@AuNP as the catalyst with time.

at time t and initial time, respectively. C_t and C_0 can also be described by the intensities of the corresponding 4-nitrophenolate ion absorption peak A_t and A_0. Hence, the plot of $\ln(A_t/A_0)$ versus time (t) shows a linear tendency (Figure 1b). k value is calculated from the early stage of the reaction for about 8 min in accordance with the previous literature,[19] to avoid the influence from side reactions occurring later.

AuNP of six different sizes from 10 to 58 nm were prepared with two different ligands, namely, citrate (Ct@AuNP) and polyvinylpyrrolidone (PVP@AuNP). Then all AuNP were investigated in the reductive reaction under the same conditions, only varying the amount of employed AuNP to keep the total surface area the same (Table S3, Supporting Information). **Figure 2**a displays the plot of $\ln(A_t/A_0)$ of reactions catalyzed by nanoparticles of different sizes. In the case of Ct@AuNP, the reductive reaction using the 58 nm AuNP provided the highest reaction rate constant (k_{TEM} = 0.10 min^{-1}). Also, the lowest rate constant was observed with the smallest 10 nm AuNP (k_{TEM} = 0.03 min^{-1}). The reaction rate showed an increasing tendency with an increase of the size of the Ct@AuNP (Figure 2c). In other words, if the total surface area ($\Sigma N_i A_i = \Sigma N_j A_j$, i and j correspond to smaller and bigger particles) was kept the same, the bigger particles provide higher catalytic activities. To further verify this observation, PVP@AuNP were prepared and employed in the reductive reaction under the same conditions. The reduction of 4-nitrophenol catalyzed by differently sized PVP@AuNP over time showed a typical induction of about 5 min, which is in good agreement with the literature[10b] (Figure 2b). Reaction rate constants using PVP@AuNP as the catalyst exhibited the same tendency as that of the Ct@AuNP (Figure 2d) (Table S3, Supporting Information). The 10 nm PVP@AuNP had the lowest catalytic activity with a k_{TEM} value of 0.052 min^{-1}. In contrast, the 58 nm PVP@AuNP had the highest catalytic activity with a k_{TEM} value of 0.11 min^{-1}. The results may hint at a higher reaction rate when using PVP@AuNP compared to Ct@AuNP.

As has been previously mentioned, the kinetic experiments were also performed in the other way, that is, the total surface area was determined by SAXS. For example, for the AuNP which are 42 nm on average in the longest dimension (TEM result) and 32 nm on average according to SAXS analysis (based on a spherical shape of the particles), we found k_{SAXS} = 0.073 min^{-1} and k_{TEM} = 0.092 min^{-1} for Ct@AuNP. For the corresponding PVP@AuNP, k_{SAXS} = 0.081 min^{-1} and k_{TEM} = 0.097 min^{-1} (Tables S3 and S4, Supporting Information). From the fact that the resulting k values are in a similar range, we conclude that even the big particles are spherical enough on average so that the equations (Figure S5, Supporting Information) can be used as an approximation.

In previous studies, the influence of the surface areas has been widely studied, and it has been well confirmed that higher surface areas result in higher catalytic reaction rate. We controlled the total surface area ($N_i A_i$) by using the equation in Figure S5 and Table S3 in the Supporting Information to calculate the required volume of colloidal solution based on the particle diameter and concentration in the different samples. By this method, our current study offers a perspective on the discussion of the catalytic behavior by comparing colloidal solution of small (N_i high) and big (N_i low) particles with identical total areas. The reaction rate increased with an increase of the size of AuNP. This result is supported by the finding of the Pal group.[11c] Based on the results mentioned above, different hypotheses were proposed in the following parts, which are assumed to affect the catalytic behavior of AuNP, namely defects within the crystalline structure, diffusion of the reactants to the catalytic surface, and ligand density on the surface of AuNP.

To investigate the influence of defects on the catalytic activity of AuNP, the crystal structures of Ct@AuNP with an average size of 10 and 42 nm were further studied by Cs-corrected TEM (**Figure 3**). Although the selected area diffraction (SAED) patterns of both Ct@AuNP on general survey images were polycrystalline (Figures S7 and S8, Supporting Information), single-crystalline and polycrystalline NP co-exists in the case of 10 nm sized Ct@AuNP, as evidenced by the high-resolution TEM (HRTEM) image (Figure 3). HRTEM images of Ct@AuNP with an average size of 42 nm show complex polycrystalline structures (Figure 3h), along with domains that do not exhibit any lattice fringes, most probably representative of amorphous regions within the AuNP. While the absence of lattice fringes is not bijective for an amorphous nature, the largely spherical form of the AuNP makes a preferential ordering with respect to the TEM grid very unlikely. The differences in the

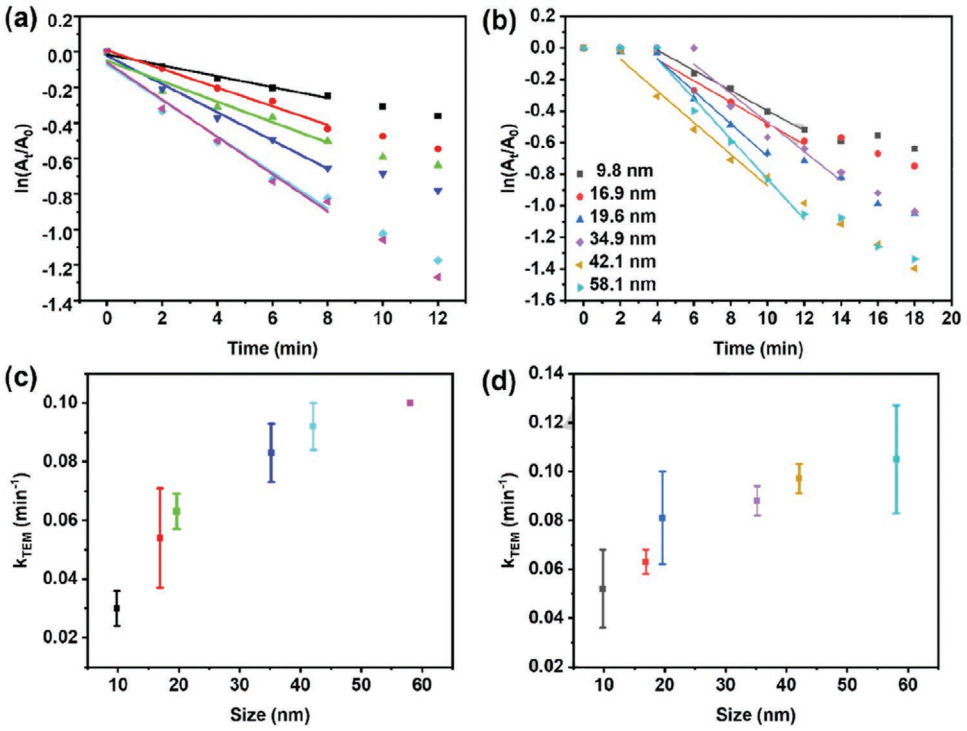

Figure 2. Kinetic study assuming a kinetic of pseudo-first order. a,b) First-order linear fitting of $\ln(A_t/A_0)$ versus time using 10–58 nm citrate and PVP capped AuNP as catalysts for the 4-nitrophenol reduction to determine k_{TEM} in Equation (1). c,d) Plot of k_{TEM} versus the size of citrate and PVP capped AuNP for the reduction of 4-nitrophenol.

crystal structure might be attributed to the different sizes of the Ct@AuNP. A recent in situ TEM study[20] revealed that NP undergo amorphous-phase-mediated crystallization, where the amorphous phase transforms into the crystalline phase. In all likelihood "capsule-like" larger NP have more remaining amorphous parts on their surface compared to smaller ones.

According to the literature,[21] generally AuNP could form face-centered-cubic (fcc) crystalline structures due to their thermodynamical stability. Typically, the major facet on the surface of the large AuNP is Au (111).[22] Thus, the marked region in Figure 3g,h may be amorphous or not. It may be explained by different crystallographic planes or defects as a result of different crystalline domains. Such defect structures include twin boundary, grain boundary, edge dislocation, screw dislocation, stepped surface, kink, and island.[23] To sum up, it seems that there are presumably more defects on the surface of the larger AuNP due to their inherent deficiencies generated from the synthetic methods.

Differences in the degree of crystallinity may go along with the size of the NP and are suggested to be one critical factor determining the overall catalytic activities (**Scheme 1**). Distortion is suggested to induce defects, which for their part influence the association or dissociation of the reagent to the surface of the AuNP, and hence the catalytic activity. Further, it has been reported that amorphous nanostructures with abundant defects exhibited higher catalytic activities compared with crystalline nanostructures.[24] In that sense, larger AuNP containing more defects have higher catalytic activities than smaller ones.

Another possible explanation for the enhanced catalytic activity of larger AuNP might be a modification of the reactant diffusion close to the catalytic surfaces, e.g., via an extension of the time that a reactant molecule remains close to the surfaces. To investigate this hypothesis, we implemented a computational algorithm to solve the convection–diffusion reaction equation using a Lattice–Boltzmann scheme (see the Experimental Section in the Supporting Information). In the simulations, either one large or two small nanoparticles are placed in a periodic box surrounded by solvent containing an initially homogeneous concentration of the reactant species A (nitrophenol). As in the experiment, $NaBH_4$ is available in excess; we implemented a first order A to B (aminophenol) reaction (with a reaction rate k) taking place whenever the reactant is in the immediate neighborhood of the nanoparticle. We compared two simulation scenarios with either one large or two small AuNP contained in a periodic box. The AuNP radii are chosen such that the total surface area is identical in both cases. A snapshot of the latter simulation is shown in **Figure 4**a.

Figure 4b shows the progress of the reaction with time for both scenarios: in contrast to the experimental observation, the reaction rate is entirely independent of the AuNP size with the simulation. Figure S9 in the Supporting Information shows that an additional hydrodynamic flow, corresponding to stirring in the experiment, does not affect this finding. We then investigated the influence of the nanoparticle surface itself on the diffusion coefficients of the reactant molecules: it is known that increasing hydrodynamic resistance slows down the diffusion

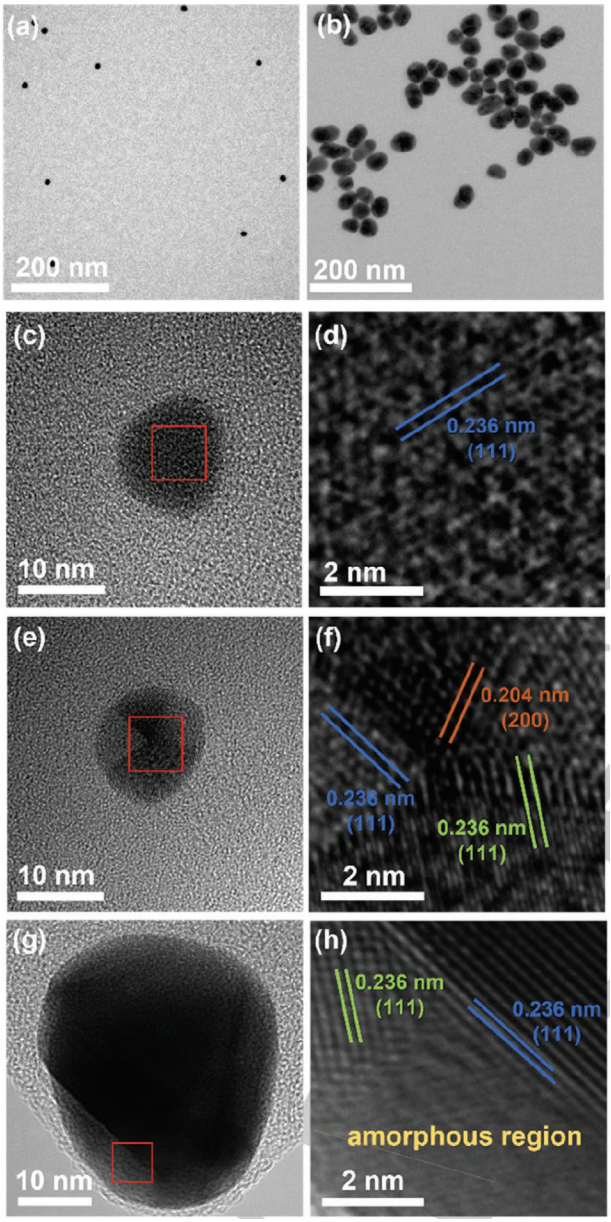

Figure 3. TEM study of Ct@AuNP. a) TEM image of 10 nm Ct@AuNP at low magnification, b) TEM image of 42 nm Ct@AuNP at low magnification, c) TEM image, and d) HRTEM image of Ct@AuNP with an average size of 10 nm showing a single crystalline structure. e) TEM image, and f) HRTEM image of Ct@AuNP with an average size of 10 nm showing polycrystalline structure. g) TEM image, and h) HRTEM image of Ct@AuNP with an average size of 42 nm showing polycrystalline and probably amorphous structures.

of molecules close to surfaces and induces an anisotropy in the system, i.e., diffusion perpendicular to the surface is slowed down more firmly than diffusion lateral to the surface. To study this effect, we used a particle model (see the Experimental Section in the Supporting Information) that accounts for anisotropic surface-modified diffusion.[25] Figure S10 in the Supporting Information shows, however, that the overall reaction efficiency is affected equally for small and large nanoparticles.

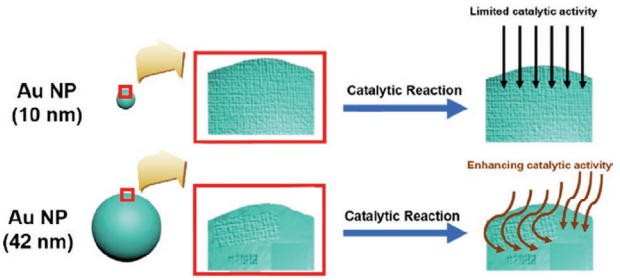

Scheme 1. Schematic illustration of the lower catalytic activities of AuNP with an average size of 10 nm compared with those of AuNP with an average size of 42 nm. The red boxes display one part of the surface of a certain AuNP.

To conclude this theoretical investigation: surface-modified diffusion of the reactant species in the proximity of the catalytic AuNP can be ruled out as an explanation for the enhancement of the overall catalytic activity of larger AuNP observed in our experiments.

Furthermore, ligands on the surface of the AuNP also have huge impact on their catalytic activities. Previously published articles have demonstrated that many parameters of the ligands can be influential, such as the functionalization and the molecule weight of the ligand.[13b,26] Hence, it is of significant importance to explore the ligand density of the AuNP within our work. Ligand density was determined according to the literature.[27] With the help of ^{1}H NMR and ICP-OES, quantitative studies of the ligand density of 10 nm 11-mercaptoundecanoic capped AuNP (MUA@AuNP) and 42 nm MUA@AuNP were carried out. Detailed procedure is described in the Experimental Section in the Supporting Information. The results indicated that the ligand densities of the AuNPs of the two different sizes were calculated to be 6.9 and 7.5 nm^{-2}, respectively. Hence, AuNP have a similar number of ligands per surface area, which is independent of the size. This result is in good agreement with literature.[27] This observation reveals that ligand density might not play an essential role in the catalytic behaviors of AuNP of different sizes.

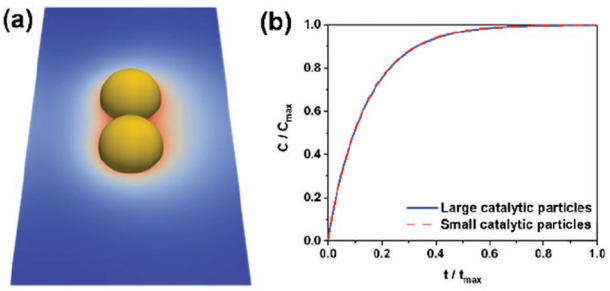

Figure 4. a) Illustration of the concentration of the product species at t/t_{max} = 0.01 for the scenario of small spheres. Red and blue lines represent high and low concentrations, respectively. b) In contrast to the experimental findings, our diffusion–reaction model suggests that large and small catalytic particles exhibit very similar catalytic activities, thus ruling out surface-modified diffusion as an explanation for the experimental findings.

3. Conclusion

In this work, Ct@AuNP ranging from 10 to 58 nm were synthesized by citrate reduction, and the corresponding PVP@AuNP were obtained via ligand exchange. Thereafter, the nitrophenol reduction reaction was performed by investigating AuNP of different sizes under the same conditions while keeping the total surface area the same. The results of catalytic reaction suggested that AuNP of different sizes with the same total surface area presented different catalytic behaviors. More defects populate on the surface of AuNP of larger size based on the result of HRTEM, which could result in more active sites distributed on their surface. This observation may provide an explanation for the size-dependent enhancement of the catalytic reaction. Our current study promotes the design of catalysts with more surface defects to facilitate and enhance the catalytic reaction. In addition, it is possible that the difference in nanoparticles' stabilities during the catalytic reaction can lead to different aggregation states of the nanoparticles, which may then influence the reaction rate. A similar amount of ligand density in the nanoparticles' solutions does not mean that the same amount of the most active sites of AuNP were occupied for nanoparticles of different sizes, which can be a potential research topic for further study.

Supporting Information

Supporting Information is available from the Wiley Online Library or from the author.

Acknowledgements

The authors acknowledge the financial support from the Deutsche Forschungsgemeinschaft (DFG, SFB 840, project B8, B9, and A12). The Bavarian Polymer Institute (BPI) is also thanked for access to the keylabs "Electron and Optical Microscopy" "Theory and Simulation" and "Mesoscale Characterization: Scattering". The work benefited from the use of the SASview application originally developed under NSP award DMR-0520547. SASview also contains code under the SINE 2020 project grant 654000.

Open access funding enabled and organized by Projekt DEAL.

Conflict of Interest

The authors declare no conflict of interest.

Data Availability Statement

The data that support the findings of this study are available in the supplementary material of this article.

Keywords

defects in gold nanoparticles, ligand density, nitrophenol reduction, polydiffusion

Received: May 31, 2021
Revised: November 8, 2021
Published online: December 16, 2021

[1] a) L. Dykman, N. Khlebtsov, *Chem.Soc. Rev.* **2012**, *41*, 2256; b) L. Cheng, C. Wang, L. Feng, K. Yang, Z. Liu, *Chem. Rev.* **2014**, *114*, 10869; c) D. A. Giljohann, D. S. Seferos, W. L. Daniel, M. D. Massich, P. C. Patel, C. A. Mirkin, *Angew. Chem., Int. Ed.* **2010**, *49*, 3280; d) C. J. Murphy, A. M. Gole, J. W. Stone, P. N. Sisco, A. M. Alkilany, E. C. Goldsmith, S. C. Baxter, *Acc. Chem. Res.* **2008**, *41*, 1721; e) E. C. Dreaden, A. M. Alkilany, X. Huang, C. J. Murphy, M. A. El-Sayed, *Chem. Soc. Rev.* **2012**, *41*, 2740.

[2] a) K. Saha, S. S. Agasti, C. Kim, X. Li, V. M. Rotello, *Chem. Soc. Rev.* **2012**, *112*, 2739; b) C. C. Huang, Z. Yang, K. H. Lee, H. T. Chang, *Angew. Chem.* **2007**, *119*, 6948; c) L. Qin, G. Zeng, C. Lai, D. Huang, P. Xu, C. Zhang, M. Cheng, X. Liu, S. Liu, B. Li, *Coord. Chem. Rev.* **2018**, *359*, 1.

[3] a) I. Venditti, *Materials* **2017**, *10*, 97; b) H. J. Kim, M. M. Hossen, A. C. Hillier, D. Vaknin, S. K. Mallapragada, W. Wang, *ACS Appl. Nano Mater.* **2020**, *3*, 8216; c) L. Shi, L. Zhu, J. Guo, L. Zhang, Y. Shi, Y. Zhang, K. Hou, Y. Zheng, Y. Zhu, J. Lv, *Angew. Chem., Int. Ed.* **2017**, *56*, 15397.

[4] a) M.-C. Daniel, D. Astruc, *Chem. Rev.* **2004**, *104*, 293; b) A. Corma, H. Garcia, *Chem. Soc. Rev.* **2008**, *37*, 2096; c) Y. Zhang, X. Cui, F. Shi, Y. Deng, *Chem. Rev.* **2012**, *112*, 2467; d) T. Ishida, T. Murayama, A. Taketoshi, M. Haruta, *Chem. Rev.* **2019**, *120*, 464; e) M. Stratakis, H. Garcia, *Chem. Rev.* **2012**, *112*, 4469.

[5] Q. He, S. J. Freakley, J. K. Edwards, A. F. Carley, A. Y. Borisevich, Y. Mineo, M. Haruta, G. J. Hutchings, C. J. Kiely, *Nat. Commun.* **2016**, *7*, 1.

[6] a) C. Shang, Z.-P. Liu, *J. Am. Chem. Soc.* **2011**, *133*, 9938; b) H. Tsunoyama, H. Sakurai, Y. Negishi, T. Tsukuda, *J. Am. Chem. Soc.* **2005**, *127*, 9374.

[7] a) T. Mitsudome, K. Kaneda, *Green Chem.* **2013**, *15*, 2636; b) A. Corma, P. Serna, *Science* **2006**, *313*, 332.

[8] J. Han, Y. Liu, R. Guo, *J. Am. Chem. Soc.* **2009**, *131*, 2060.

[9] H. Zhu, X. Ke, X. Yang, S. Sarina, H. Liu, *Angew. Chem., Int. Ed.* **2010**, *49*, 9657.

[10] a) P. Zhao, X. Feng, D. Huang, G. Yang, D. Astruc, *Coord. Chem. Rev.* **2015**, *287*, 114; b) S. Wunder, Y. Lu, M. Albrecht, M. Ballauff, *ACS Catal.* **2011**, *1*, 908.

[11] a) S. Panigrahi, S. Basu, S. Praharaj, S. Pande, S. Jana, A. Pal, S. K. Ghosh, T. Pal, *J. Phys. Chem. C* **2007**, *111*, 4596; b) R. Fenger, E. Fertitta, H. Kirmse, A. F. Thünemann, K. Rademann, *Phys. Chem. Chem. Phys.* **2012**, *14*, 9343; c) T. K. Sau, A. Pal, T. Pal, *J. Phys. Chem. B* **2001**, *105*, 9266; d) X. Zhou, W. Xu, G. Liu, D. Panda, P. Chen, *J. Am. Chem. Soc.* **2010**, *132*, 138; e) J. Piella, F. Merkoçi, A. Genç, J. Arbiol, N. G. Bastús, V. Puntes, *J. Mater. Chem. A* **2017**, *5*, 11917.

[12] S. Kundu, S. Lau, H. Liang, *J. Phys. Chem. C* **2009**, *113*, 5150.

[13] a) S. Satapathy, J. Mohanta, S. Si, *ChemistrySelect* **2016**, *1*, 4940; b) S. M. Ansar, C. L. Kitchens, *ACS Catal.* **2016**, *6*, 5553.

[14] P. Suchomel, L. Kvitek, R. Prucek, A. Panacek, A. Halder, S. Vajda, R. Zboril, *Sci. Rep.* **2018**, *8*, 1.

[15] G. Frens, *Nat. Phys. Sci.* **1973**, *241*, 20.

[16] A. Avellan, J. Yun, Y. Zhang, E. Spielman-Sun, J. M. Unrine, J. Thieme, J. Li, E. Lombi, G. Bland, G. V. Lowry, *ACS Nano* **2019**, *13*, 5291.

[17] S. Gu, S. Wunder, Y. Lu, M. Ballauff, R. Fenger, K. Rademann, B. Jaquet, A. Zaccone, *J. Phys. Chem. C* **2014**, *118*, 18618.

[18] S. Wunder, F. Polzer, Y. Lu, Y. Mei, M. Ballauff, *J. Phys. Chem. C* **2010**, *114*, 8814.

[19] P. Herves, M. Pérez-Lorenzo, L. M. Liz-Marzán, J. Dzubiella, Y. Lu, M. Ballauff, *Chem. Soc. Rev.* **2012**, *41*, 5577.

[20] J. Yang, J. Koo, S. Kim, S. Jeon, B. K. Choi, S. Kwon, J. Kim, B. H. Kim, W. C. Lee, W. B. Lee, H. Lee, T. Hyeon, P. Ercius, J. Park, *J. Am. Chem. Soc.* **2019**, *141*, 763.

[21] a) Z. Fan, X. Huang, Y. Chen, W. Huang, H. Zhang, *Nat. Protoc.* **2017**, *12*, 2367; b) P. Nayebi, E. Zaminpayma, *J. Cluster Sci.* **2009**, *20*,

661; c) J.-H. Shim, S.-C. Lee, B.-J. Lee, J.-Y. Suh, Y. W. Cho, *J. Cryst. Growth* **2003**, *250*, 558.

[22] a) A. S. Barnard, *Acc. Chem. Res.* **2012**, *45*, 1688; b) J.-W. Park, J. S. Shumaker-Parry, *J. Am. Chem. Soc.* **2014**, *136*, 1907; c) A. S. Barnard, N. P. Young, A. I. Kirkland, M. A. Van Huis, H. Xu, *ACS Nano* **2009**, *3*, 1431.

[23] S. K. De, S. Mondal, P. Sen, U. Pal, B. Pathak, M. Bardhan, M. Bhattacharya, B. Satpati, A. De, D. Senapati, *Nanoscale* **2018**, *10*, 11091.

[24] a) P. Pal, R. K. Singha, A. Saha, R. Bal, A. B. Panda, *J. Phys. Chem. C* **2015**, *119*, 13610; b) Y. Ma, R. Wang, H. Wang, V. Linkov, S. Ji, *Phys. Chem. Chem. Phys.* **2014**, *16*, 3593; c) C.-S. Kuo, C.-R. Kao, W.-J. Chen, M.-Y. Lu, D. A. Cullen, B. T. Sneed, Y.-C. Chuang, C.-C. Yu, C.-H. Kuo, *Chem. Mater.* **2018**, *30*, 4448; d) K. Rossi, G. G. Asara, F. Baletto, *ACS Catal.* **2020**, *10*, 3911.

[25] a) A. J. Goldman, R. G. Cox, H. Brenner, *Chem. Eng. Sci.* **1967**, *22*, 637; b) A. Daddi-Moussa-Ider, A. Guckenberger, S. Gekle, *Phys. Rev. E* **2016**, *93*, 012612.

[26] a) R. D. Neal, R. A. Hughes, P. Sapkota, S. Ptasinska, S. Neretina, *ACS Catal.* **2020**, *10*, 10040; b) S. Roy, A. Rao, G. Devatha, P. P. Pillai, *ACS Catal.* **2017**, *7*, 7141.

[27] A. M. Smith, L. E. Marbella, K. A. Johnston, M. J. Hartmann, S. E. Crawford, L. M. Kozycz, D. S. Seferos, J. E. Millstone, *Anal. Chem.* **2015**, *87*, 2771.